

# Membrane Mechanical Properties Regulate the Effect of Strain on Spontaneous Electrophysiology in Human iPSC-Derived Neurons

Fabio Bianchi, Valerio Pereno, Julian H. George, Mark S. Thompson and Hua Ye\*

*Institute of Biomedical Engineering, Dept. of Engineering Science, University of Oxford, Oxford OX3 7DQ, UK*

**Abstract**—Peripheral nerves contain neuron fibers vital for movement and sensation and are subject to continuous elongation and compression during everyday movement. At supraphysiological strains conduction blocks occur, resulting in permanent or temporary loss of function. The mechanisms underpinning these alterations in electrophysiological activity remain unclear; however, there is evidence that both ion channels and network synapses may be affected through cell membrane transmitted strain. The aim of this work was to quantify the changes in spontaneous activity resulting from application of uniaxial strain in a human iPSC-derived motor neuron culture model, and to investigate the role of cell membrane mechanical properties during cell straining. Increasing strain in a custom-built cell-stretching device caused a linear decrease in spontaneous activity, and no immediate recovery of activity was observed after strain release. Imaging neuronal membranes with c-Laurdan showed changes to the lipid order in neural membranes during deformation with a decrease in lipid packing. Neural cell membrane stiffness can be modulated by increasing cholesterol content, resulting in reduced stretch-induced decrease of membrane lipid packing and in a reduced decrease in spontaneous activity caused by mechanical strain. Together these results indicate that the mechanism whereby cell injury causes impaired transmission of neural impulses may be governed by the mechanical state of the cell membrane, and contribute to establishing a direct relationship between neural uniaxial straining and loss of spontaneous neural activity. © 2019 The Author(s). Published by Elsevier Ltd on behalf of IBRO. This is an open access article under the CC BY license (<http://creativecommons.org/licenses/by/4.0/>).

**Key words:** electrophysiology, cholesterol, lipid packing, neural damage, calcium imaging, uniaxial strain.

## INTRODUCTION

During mechanical injury to the nervous system, multi-scale partitioning of strains and stresses results in cell deformation, which in turn affects cellular function (Ng et al., 2017). In peripheral nerves, conduction blocks are observed following supraphysiological extension of 5–20% (Rickett et al., 2011) and strain rates as low as 0.008% (Shi and Whitebone, 2006), suggesting induced electrophysiological dysfunction. In white matter, tissue strain has been shown to affect axons and cell bodies at the microscopic level (Bain and Meaney, 2000; Singh et al., 2017), but the mechanisms that lead to impaired electrical activity are not fully understood. The wide range of putative injury mechanisms points to multi-scale alterations, from aberrant synaptic connectivity to dysfunctional electrophysiological mechanisms in individual cells.

Network electrophysiological activity is initiated from synaptic connection between functional neurons, and is known to be vulnerable to mechanical insult (Sharp et al., 2014). Using a shear-flow injury model coupled with multi-electrode array recordings, Prado et al. have shown that mechanical injury causes partial or complete cessation of spontaneous electrical activity in cultured cortical rat neurons, linking it with increased membrane permeability (Prado et al., 2005). Magou et al. assessed changes in network activity from rat neocortical neurons by patch clamping, showing dramatically decreased firing rates 30 min after injury (60% strain at 30 s<sup>-1</sup> strain rate) and concurrent hyperexcitability of non-injured neurons within injured cultures, indicating aberrant synaptic connectivity (Magou et al., 2015). Goforth et al. showed, by calcium imaging and spontaneous and miniature post-synaptic currents, that injury decreases spontaneous calcium oscillations and depressed post-synaptic currents, again indicating a direct effect of injury on network connectivity (Goforth et al., 2011).

Ion channels, the transmembrane proteins responsible for the regulation of membrane potential and for the initiation and propagation of action potentials (APs), are embedded in the cell membrane, and are known to be finely

\*Corresponding author. Tel.: +44 1865 617689.

E-mail address: [hua.ye@eng.ox.ac.uk](mailto:hua.ye@eng.ox.ac.uk)

**Abbreviations:** AP, action potential; GP, generalised polarisation; MβCD, methyl-β-cyclodextrin; iPSC, induced pluripotent stem cells; PDMS, polydimethylsiloxane; DAPI, 4',6-diamidino-2-phenylindole; FITC, Fluorescein isothiocyanate; FIJI, Fiji Is Just ImageJ; DMEM, Dulbecco's Modified Eagle Medium; FB-DMEM, FluoroBrite-Dulbecco's Modified Eagle Medium; ANOVA, Analysis of variance.

mechanosensitive (Tyler, 2012; Anishkin et al., 2014). The forces regulating ion channel gating originate from the surrounding lipid membrane, suggesting a close relationship between membrane mechanics and electrophysiological activity (Lundbæk et al., 1996; Phillips et al., 2009). For example, membrane stiffening by stomatin-like protein-3 (STOML3) has been shown to finely control mechanically gated ion channel activity in sensory neurons (Qi et al., 2015). This is not limited to mechanosensitive channels, as voltage- and ligand-gated channels have also been shown to be variably mechanosensitive, and their activity altered by localized membrane suction (Lundbæk et al., 2004; Laitko et al., 2006; Wang et al., 2009; Morris et al., 2015). The cell membrane has further been implicated in neural mechanical damage, which leads to membrane poration and increased permeability (Geddes et al., 2003; Prado et al., 2005; LaPlaca et al., 2018).

Cholesterol, physiologically accounting for approximately half of the cell membrane by molar fraction, can be used to modify membrane mechanical properties (Needham and Nunn, 1990). Cholesterol level can be manipulated by addition of methyl- $\beta$ -cyclodextrin (M $\beta$ CD); addition of unloaded M $\beta$ CD causes depletion of cholesterol from cell membranes, whereas cholesterol-loaded M $\beta$ CD enriches cholesterol content (Christian et al., 1997). In turn, this alters the mechanical properties of the membrane (Needham and Nunn, 1990; Yang et al., 2011; Al-Rekabi and Contera, 2018), and affects synaptic activity (Koudinov and Koudinova, 2001; Zamir and Charlton, 2006) and the function of transmembrane proteins including ion channels (Spector and Yorek, 1985; Tillman and Cascio, 2003; Barrantes, 2004; Levitan et al., 2010). The effects of membrane stretch and cholesterol depletion are strikingly similar. Both cause accelerations in ion channel current time-course, decrease in current amplitude, alterations in APs (Guo et al., 2008), and blocking of synaptic transmission in networks (Zamir and Charlton, 2006). This remarkable resemblance suggests that both processes affect ion channel and synaptic function by altering the mechanical environment of the cell membrane. Currently, no study has investigated the role of membrane mechanical properties on the consequences of strain applied to neurons.

The aim of this study was to quantify the changes in spontaneous activity in cultures of human iPSC-derived neurons subject to uniaxial strain, and how changing the membrane mechanical properties affect cells subject to strain. Using a custom-built substrate-straining device we applied uniaxial strain to human iPSC-derived neurons with and without cholesterol addition, and recorded activity using calcium imaging. To quantify the effect of stretch and cholesterol addition on the mechanical properties of the membrane, we use c-Laurdan spectral imaging to quantify membrane lipid packing.

Understanding the mechanisms of electrophysiological dysfunction in neurons and the importance of membrane mechanical properties during cell deformation can provide useful insights on the mechanisms underlying conduction blocks in peripheral sensory and motor tracts, aiding the development of protective and restorative strategies and the understanding of heightened neural vulnerability following sub-lethal injury.

## MATERIALS AND METHODS

### Cell Culture

Human motor neurons were differentiated from induced pluripotent stem cells (iPSC) obtained through StemBANCC, Oxford, following a previously established protocol (Bianchi et al., 2018). Following differentiation by dual-SMAD inhibition and differentiation to motor neuron lineage, neurons were matured for a minimum of 21 days in media consisting of 50% knockout-Dulbecco's modified eagle medium:F12 (KO-DMEM:F12 ThermoFisher, UK) and 50% neurobasal medium (ThermoFisher, UK), supplemented with 1% penicillin streptomycin (P/S, Sigma-Aldrich, UK), 1% B27 (ThermoFisher, UK), 1% N2 (ThermoFisher, UK), 1% nonessential amino acids (ThermoFisher, UK), 1% glutaMAX (ThermoFisher, UK), 0.1 mM L-ascorbic acid (Sigma-Aldrich, UK), 10 ng/ml ciliary neurotrophic factor (Peprotech, UK), 10 ng/ml brain derived neurotrophic factor (BDNF, Peprotech, UK), 10 ng/ml NT-3 (Peprotech, UK), and 10 ng/ml glia derived neurotrophic factor (GDNF, Peprotech, UK).

### Cell Stretching

Cells were deformed using a custom-built substrate stretching device (Fig. 1), delivering uniaxial strain to cells cultured on ultrathin (50–100  $\mu$ m) polydimethylsiloxane (PDMS) substrates (Silex, UK) and allowing for simultaneous high-resolution microscopy and electrophysiological recording (Wei et al., 2018). iPSC-derived neurons were seeded on deformable substrates at 30,000 cells/substrate.

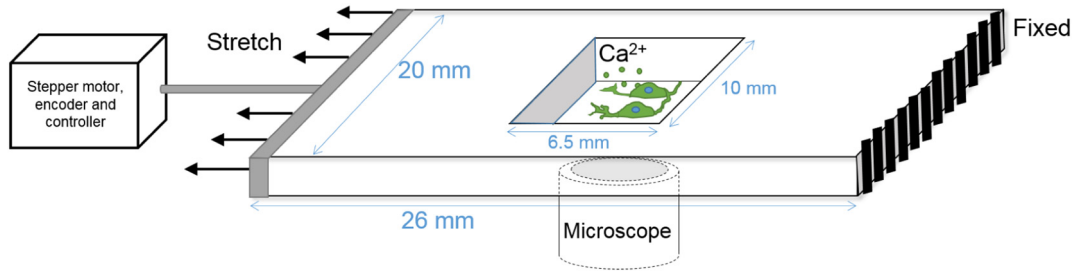
Neurons were subjected to graded strain applications, from 0% (unstretched) to 25%, 45% and 75% strain and released back to 0%, all carried out at 0.1 s<sup>-1</sup> strain rate (Fig. 2). At each strain point time-lapse imaging of intracellular calcium concentration was recorded for 4 min. The same stretch protocol was repeated for cell samples loaded with cholesterol and for c-Laurdan lipid packing imaging.

### Live Cell Staining and Strain Measurement

Cell membranes were stained using cellmask green (ThermoFisher, UK) live cell dye, at 1:1000 concentration, for 5 min at 37 °C. Nuclei were stained using nucblue (ThermoFisher, UK) at 2 drops/ml, for 15 min at 37 °C. Images were taken using a Nikon Ti-E inverted fluorescence microscope (20 $\times$  lens) using standard DAPI and FITC filters (360/460 and 490/520 nm excitation/emission). Nucleus morphology was measured using Ovuscul, a FIJI (NIH, USA) plugin which fits an ellipse to areas of high contrast and returns major and minor axis measurements (Thévenaz et al., 2011). Membrane strain was measured manually by using distinct membrane features as markers and measuring lengths along cell major and minor axis, and calculating strain as  $\epsilon = \frac{L_s - L_o}{L_o}$  where  $L_s$  and  $L_o$  are the stretched length and original length, respectively.

### Membrane Cholesterol Addition

Membrane cholesterol levels were increased by addition of water-soluble cholesterol in methyl- $\beta$ -cyclodextrin saturated



## C-Laurdan Imaging

The lipid organization of the cell membrane, commonly referred to as lipid packing, was calculated from the red- or blue-shift emission of a polarity-sensitive probe using c-Laurdan, a spectral imaging microscopy

technique described previously (Sezgin et al., 2014; Pereno et al., 2017).

The neurons were labeled with c-Laurdan (SFC, Chunbuk, Republic of Korea), at a final concentration of 400 nM in fluorobrite-DMEM imaging media (FB-DMEM, ThermoFisher, UK), immediately prior to imaging. The cell sample was then excited with a 405-nm laser and imaged using a Zeiss 710 confocal microscope equipped with a 32-channel GaAsP detector array (Fig. 3). The intensity of the emission spectrum was detected and recorded in the 415–691-nm range.

The emission spectrum of c-Laurdan is related to the dipolar water relaxation in the proximity of the probe, indicating the degree of hydration within its surrounding micro-environment. This, in turn, is indicative of the lipid packing of the plasma membrane. Generalized polarization (GP), a well-established parameter for quantification of membrane hydration, was used to quantify the relative degree of lipid packing on a scale of –1 to 1, where –1 represents the most hydrated (least packed, most fluidized) and +1 represents the least hydrated (most packed, least fluidized) membrane state. GP was calculated by comparing the intensity of the emission at two specific wave-

lengths, 440 ( $I_{440}$ ) and 490 nm ( $I_{490}$ ) as  $GP = \frac{I_{440} - I_{490}}{I_{440} + I_{490}}$ . GP was calculated for cells before, during and after stretch, both with and without addition of soluble cholesterol. An automated MATLAB script was used to select image areas containing cells, segment cell profiles, isolate cell membranes, and calculate GP values (Aron et al., 2017).

## Functional Calcium Imaging and Analysis

Calcium imaging was used to probe the intracellular calcium

**Fig. 1.** Experimental setup for cell straining. Neurons cultured on deformable PDMS substrates were subjected to uniaxial strains, and spontaneous activity measured by calcium imaging using an inverted fluorescence microscope.

complexes (CH-M $\beta$ CD, 4% Cholesterol content (w/w), Sigma-Aldrich, UK) in culture medium at a final concentration of 200  $\mu$ M. Cells were incubated 30 min prior to experiments. Saturated CH-M $\beta$ CD complexes have been shown to act as efficient cholesterol donors towards cell membranes, when added to culture medium at this concentration (Christian et al., 1997; Zidovetzki and Levitan, 2007; Guo et al., 2008).

Cholesterol addition was assessed by filipin III staining. Cells, both cholesterol loaded and control, were fixed in 4% paraformaldehyde (Sigma-Aldrich, UK) in phosphate buffered saline (PBS, ThermoFisher, UK), for 20 min at room temperature. Filipin III (Santa Cruz Biotechnologies, USA) was dissolved in dimethylsulfoxide (DMSO, Sigma-Aldrich, UK) and added to cell medium at a final concentration of 50  $\mu$ g/ml. Cells were incubated for two hours at room temperature and imaged using standard DAPI filters (360/460 nm excitation/emission) using the same acquisition settings for control and cholesterol-loaded cells, and fluorescence intensity normalized by cell body area was measured in FIJI.

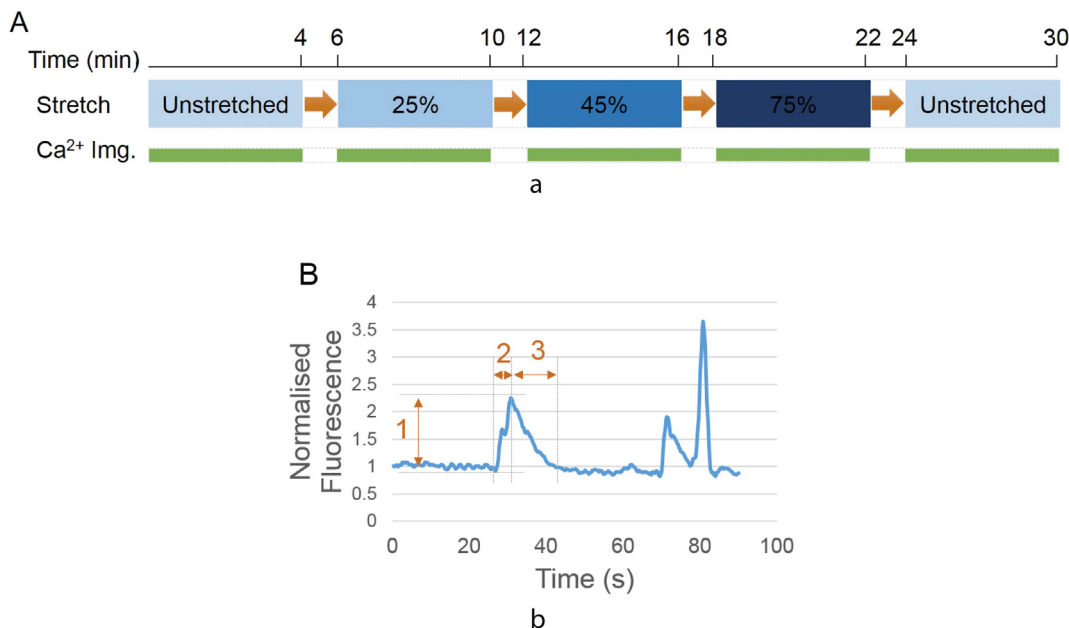


**Fig. 2.** (A) Typical strain and calcium imaging protocol, with graded increase in applied stretch, and four minutes calcium imaging at each condition. Orange arrows represent time during which strain is being applied. (B) Representative Calcium imaging trace, showing spike magnitude (1), rise time (2) and fall time (3) measurements.

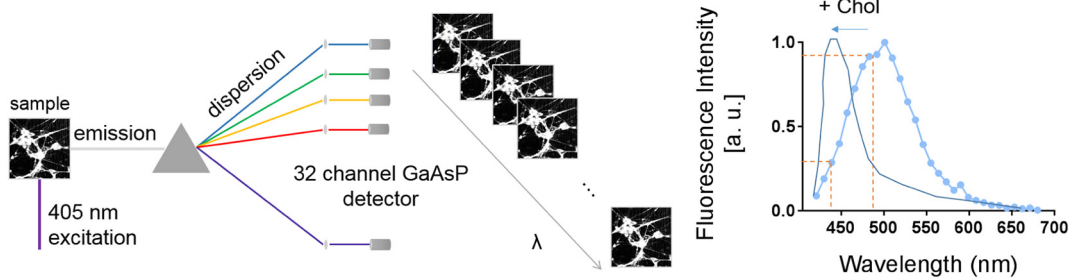


**Fig. 3.** Spectral imaging acquisition for c-Laurdan imaging. The stained sample (left) was excited with 405 nm laser, and emitted light was dispersed and detected by a 32-channel GaAsP detector, where each channel detects a specific wavelength (middle). Fluorescence intensity was plotted as a function of emission wavelength, and  $I_{440}$  and  $I_{490}$  are used to calculate generalized polarization (GP). Green profile indicates shift caused by cholesterol addition. Adapted, with permission, from (Sezgin et al., 2015).

concentration of multiple spontaneously active cells. Rapid increases in intracellular calcium concentration are associated with pre- and post-synaptic activity, therefore acting as an indirect marker of spontaneous electrophysiological activity (Grienberger and Konnerth, 2012). Imaging of intracellular free calcium was carried out using Oregon Green 488 BAPTA-1 (OGB1, Thermo Fisher, UK). A stock solution of the dye was made by dissolving OGB1 in DMSO containing 20% Pluronic F-127 (Sigma Aldrich, UK), used to avoid dye compartmentalization within the cell (Smetters et al., 1999). The solution was first brought to a 1-mM concentration by addition of PBS and a then to 20  $\mu$ M (stock solution), by further addition of PBS. Solution was sonicated for 5 min after each step. A 2- $\mu$ M working solution was made by addition of FB-DMEM, a high-glucose medium formulated to reduce background fluorescence during imaging, with a free calcium content (1.8 mM) suitable for intracellular calcium recordings (Simons, 1988). Cells were loaded with dye solution for 30 min at 37 °C washed in PBS, and incubated for a further 30 min in fresh FB-DMEM. Cells were then imaged using time-lapse microscopy, on a Nikon Ti-E microscope (10 $\times$  lens), at 10 frames per second for four minutes for unstretched and stretched conditions (Fig. 1). Regions of interest were drawn around cell bodies and background, and fluorescent intensity plotted over time. A custom-written MATLAB code was used to subtract background readings, filter traces, normalize traces by the fluorescence at  $t = 0$ , plot all traces, identify calcium spikes (by identifying rapid increases in fluorescence (> 5%)), then manually verified to avoid including artefacts) and measure spike magnitude, rise time as time from baseline to maximum, and fall time (as time from maximum back to baseline) (Fig. 2). Active cells were defined as those showing at least one rapid spike in fluorescence. Activity was measured as the percentage of active cells, and expressed normalized by the value for unstretched cells.

### Statistical Analysis

Statistical analysis was carried out in PRISM v6 (Graphpad, USA). Data were tested for significance using two-way ANOVA testing with Tukey's multiple comparisons, or by paired or unpaired student  $t$ -test (for any experiment involving

two conditions, measured from the same (paired) or different (unpaired) samples). All data are reported as mean  $\pm$  standard deviation.

## RESULTS

### Strain in Neuron Membranes and Nuclei

To determine the localization of applied

deformation, strains were measured in individual cell membranes and nuclei. Human iPSC-derived neurons show a hierarchical strain partitioning, with average membrane deformation found to be significantly higher than nucleus deformation, for all magnitudes of applied strain (Fig. 4). Average strain in both nuclei and membranes increased with increasing substrate strain, confirming good adhesion between the deformable substrate and the cells. On average, 70% of the applied substrate strain is transferred to the membrane, and 25% to the nucleus, in line with previously reported strain transfer ratios in cells cultured on elastic substrates (Wall et al., 2007).

### Effects of Strain and Cholesterol Addition on Membrane Lipid Packing

GP of neuron membranes was measured by imaging cells stained with c-Laurdan. GP decreased significantly with increasing applied strain in control cells (Fig. 5A), indicating

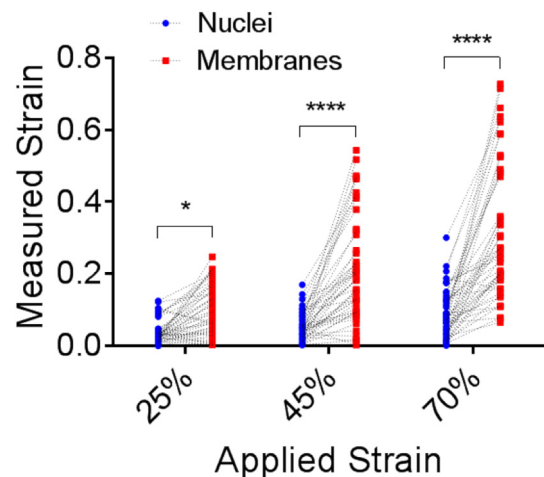


**Fig. 4.** Strain in cell membranes and nuclei. For three applied substrate strains (25%, 45% and 70%), magnitude of deformation of individual cell membranes is higher than deformation of nuclei.  $n = 49$  cells from three independent samples. Grey dotted lines show nucleus and membrane strain from the same cells. (\*\*\*\* $p < 0.0001$ , \* $p = 0.0169$  by two-way ANOVA with Tukey's multiple comparison between each applied strain level,  $n = 49$  cells).



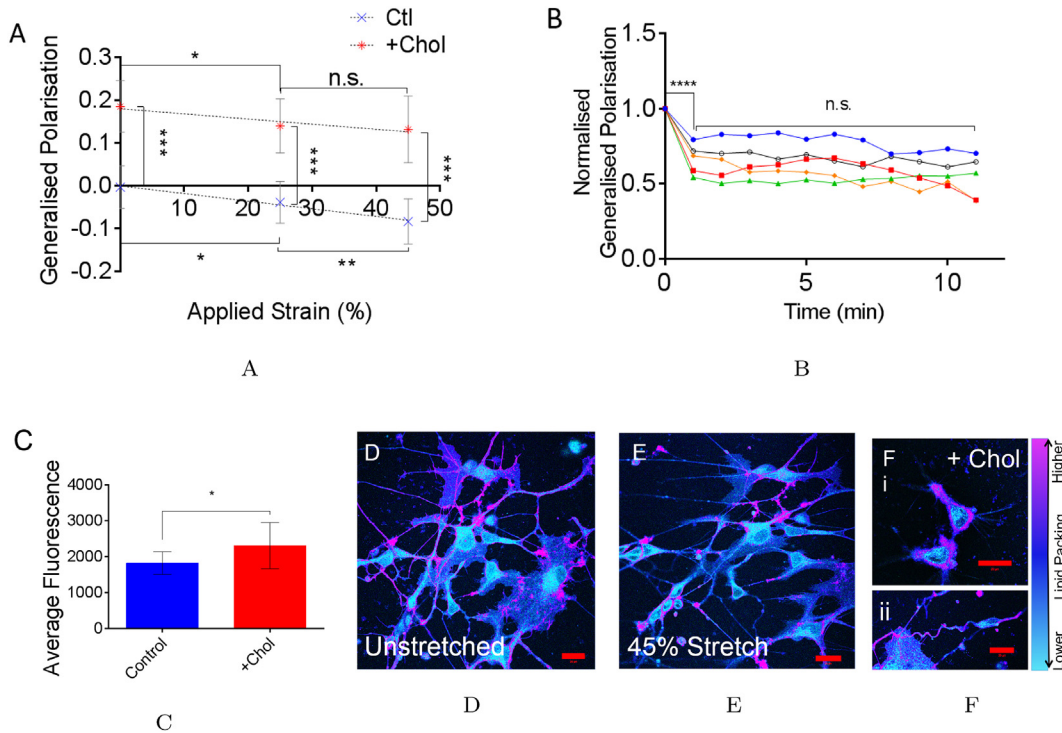


**Fig. 5.** (A) Generalized Polarization (GP) of segmented membranes from multiple cells per image, subject to increasing strain (0%, 25% and 45%), in control cells ('Ctl') and with cholesterol addition ('+Chol'). Cholesterol increases GP in unstretched and strained cells (\*\*\*\* $p < 0.0001$  (at 45%), \*\*\* $p = 0.0003$  (at 0%) and \*\*\* $p = 0.0006$  (at 25%)  $n = 6$  per group, unpaired  $t$ -test to compare between 'Ctl' and '+Chol' groups at each applied strain level). Strain induces fluidization in control cells (\* $p = 0.0103$ , \*\* $p = 0.0018$ ,  $n = 6$  per group, paired one-way ANOVA with Tukey's multiple comparisons to compare between applied strain level within 'Ctl' samples) and in cholesterol-enriched cells (\* $p = 0.0213$ , n.s. = not significant,  $n = 6$  per group, paired one-way ANOVA with Tukey's multiple comparisons to compare between applied strain level within '+Chol' samples). Minimum three cells per  $n$  in each group. (B) Time-measurements of GP, with 45% strain applied after 1 min. (\*\*\*\* $p < 0.0001$ , n.s.  $p > 0.05$  by paired  $t$ -test between timepoints for each sample.  $n > 5$  cells per sample). (C) Quantification of average fluorescence intensity from filipin staining. \* $p = 0.0354$  by unpaired  $t$ -test. (D–E) C-Laurdan spectral imaging of unstretched and 45% strained human iPSC neurons (without cholesterol addition). (F) Effect of cholesterol addition (i) and change in axonal geometry (without cholesterol addition) following stretch (ii). Purple areas qualitative show regions with higher lipid packing (color scale for reader clarity only, not quantitative). Scale bars = 20  $\mu\text{m}$ .

a decrease in lipid packing at the cell membrane. To control for dye photobleaching, time-series imaging of c-Laurdan stained neurons was performed. Following an initial decrease due to stretch, GP remained constant for ten minutes, confirming no significant photobleaching effect (Fig. 5B).

Cholesterol content of iPS-derived neuron membranes was increased by incubation with cholesterol-loaded M $\beta$ CD for 30 min, and confirmed by filipin staining (Fig. 5C). Addition of cholesterol increased baseline GP, indicating an increase in membrane lipid packing. In cholesterol-enriched cells the fluidization (decrease in lipid packing) effect of strain appeared less pronounced especially at higher strains. Average GP did not change significantly between 25% and 45% strain in cholesterol-enriched cells, but decreased significantly in control cells. Average slope of linear segments between 25% and 45% strain was significantly lower in cholesterol enriched cells. The effect of adding cholesterol was qualitatively visualized in lambda stack images, where an increase in red-shifted areas indicated higher lipid packing (Fig. 5D, E and F (i)).

## Effects of Strain and Cholesterol Addition on Spontaneous Activity

Base activity, defined as percentage of active cells before stretching, remained unchanged following addition of cholesterol (Fig. 6A).

To measure the effect of mechanical deformation on spontaneous activity, mature human iPS-derived neuronal cultures ( $N = 7$ , 83 cells average per  $N$ ) were subject to increasing strains of up to 75% with calcium activity recorded at each strain level. Measurements immediately after strain release were used to assess immediate recovery. Cell calcium activity decreased significantly when strain was applied, proportionally to applied strain (Fig. 6B). After applying 25% strain, activity decreased by

half. At 45% strain, the percentage of active cells decreased to 30%, further decreasing to 7% at 75% applied stretch. After release, no immediate recovery was found, instead a near-complete silencing of spontaneous calcium spiking was observed. A significantly smaller reduction in number of active cells was observed in cholesterol-enriched cells for each level of applied strain (Fig. 6B), including after strain release.

Calcium spiking rise time (time from baseline to spike peak) and fall time (time from spike peak back to baseline) were both significantly increased by a factor of two at 25% applied strain (Fig. 6C and D), and did not change with further strain. Rise and fall time of calcium spikes for cells with increased membrane cholesterol was not significantly altered by strain (Fig. 6C and D).

The number of spikes per active cell, indicating spiking frequency, significantly decreased from 2.75 to 1.2 with increasing strain (Fig. 6E). The number of spikes per active cells decreased less in cholesterol-enriched cells compared to control cells, with a significant decrease only at 45% applied strain (Fig. 6E).

No significant change in spike magnitude was observed between control cells and cholesterol-loaded cells, for all

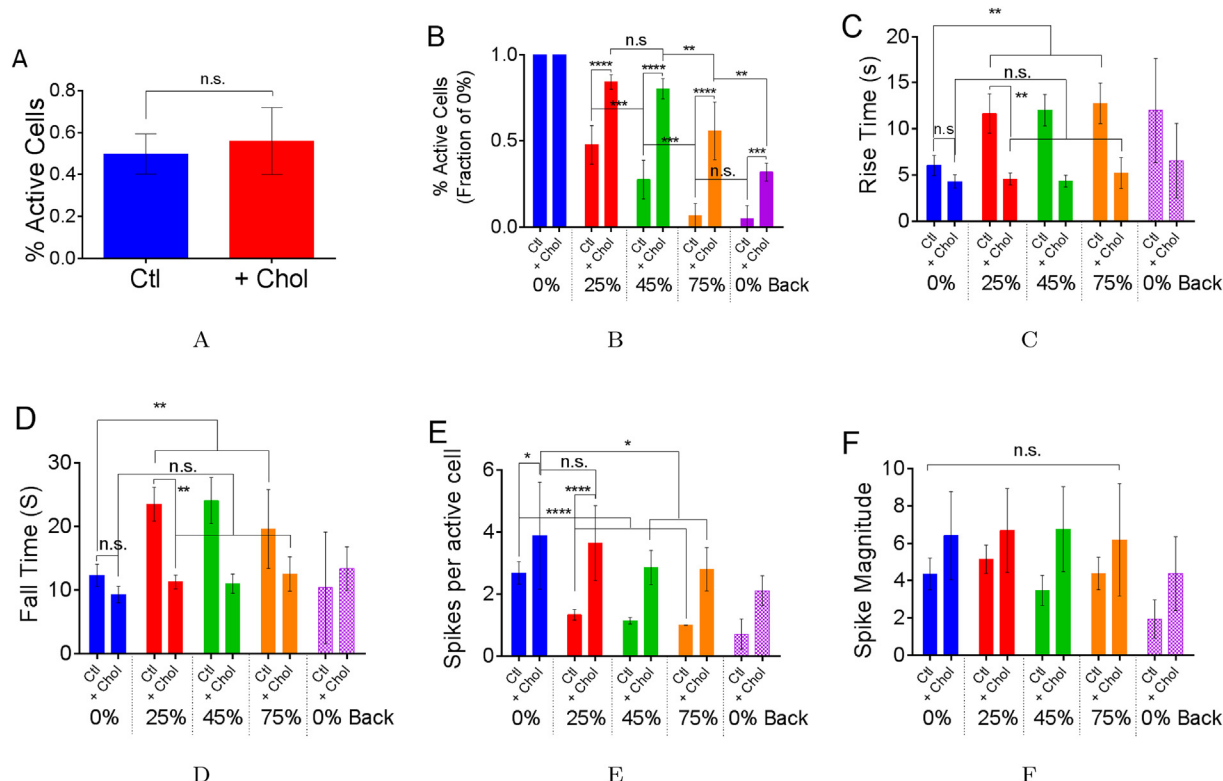


**Fig. 6.** Changes in spontaneous calcium activity with applied deformation for cholesterol-enriched cells. (A) Basal spontaneous activity is not significantly affected by addition of cholesterol (n.s. =  $p > 0.05$  by unpaired t-test). (B) Spontaneous activity (percentage active cells), normalised by the unstrained value for each condition (\*\*\*\* $p < 0.0001$  between Ctl and +Chol at strain conditions. n.s.  $p > 0.05$ . \*\*\* $p = 0.0002$  for Ctl between 25% and 45% strain and 0.0001 for Ctl between 45% and 75% strain. \*\* $p = 0.0042$  for +Chol between 45% and 75% and 0.0054 for +Chol between 75% and 0% Back). (C) Spike rise time (\*\* $p = 0.0046$ , 0.0021, 0.0046 between unstrained and 25%, 45% and 70% in control cells, \*\* $p = 0.0026$  for 25% strained cells between Ctl and +Chol, n.s.  $p = > 0.05$  between strain levels for +Chol cells, and for unstrained cells between Ctl and +Chol). (D) Spike fall time (\*\*\*\* $p = 0.0003$ , 0.0002, 0.0005 between unstrained and 25%, 45% and 70% in control cells, \*\* $p = 0.0044$  for 25% strained cells between Ctl and +Chol, n.s.  $p = > 0.05$  between strain levels for +Chol cells, and for unstrained cells between Ctl and +Chol). (E) Average number of spikes per active cell (\*\*\*\* $p < 0.0001$ , n.s.  $p = > 0.05$  between unstrained and 25%, \* $p = 0.0450$ , 0.0312 between unstrained and 45% and 70%. \* $p = 0.0223$  for unstrained cells, between Ctl and +Chol, \*\*\*\* $p < 0.0001$  for 25% strain, between Ctl and +Chol). (F) Average spike magnitude (n.s.  $p > 0.05$ ).

strain conditions (Fig. 6F). In control cells, spike magnitude (percentage increase with respect to baseline) did not change between increasing strains, but decreased when strain was released (Fig. 6F).

Rise and fall time, number of spikes per cell and spike magnitude values for cells immediately after strain release were not included in analysis due to the low number of active cells and are shown by shaded bars.

## DISCUSSION

The aim of this work was to quantify the changes in spontaneous activity of human iPSC-derived neurons subject to uniaxial strain, and to investigate the role of cell membrane mechanical properties in regulating the effects of stretch on neurons.

### Cell Membrane Strain and Lipid Packing

The transfer of strain from the deformable substrate to the cell membrane and nucleus was measured in iPSCs subject to 25%, 45% and 70% substrate strain. Results showed that a larger percentage of substrate strain was transferred to the

membrane compared to the nucleus. Previous studies hypothesized that this is due to higher nuclear stiffness, and to indirect or incomplete cytoskeletal mechanical linking to the nucleus (Gilchrist et al., 2007). Evidence of ion channel mechanosensitivity in cytoskeleton-depleted cells and in reconstructed artificial bilayers (Brohawn et al., 2014) points to the membrane regulating the mechanical environment to which transmembrane proteins are exposed. The higher membrane strains measured suggest that the membrane mechanical environment is significantly altered during cell stretch, and that functional changes may therefore arise as a direct consequence of membrane deformation.

To quantify the effect of strain on the membrane, changes in lipid packing during cell straining were measured using c-Laurdan, a polarity-sensitive probe which produces a red or blue shifted signal depending on membrane hydration level (Sezgin et al., 2014; Pereno et al., 2017). This technique has, to the best of our knowledge, never been applied to study structural changes of neural membranes subject to deformation. Applying strain to human iPSC-derived neurons caused a decrease in generalized polarization (GP), indicating a decrease in lipid packing (increase in membrane

fluidity) (Fig. 5, blue bars). Intuitively, stretch reduces the lateral packing density of membrane elements. In endothelial cells, GP has been shown to increase during stretch and decrease under fluid shear stress (Yamamoto and Ando, 2013), a response thought to be due to cell specialization in differentiating between mechanical stimuli (Yamamoto and Ando, 2015). In neurons, which are not required to differentiate between mechanical stimuli, the measured decrease in membrane lipid packing shows that the membrane state is directly altered by strain.

Increasing cholesterol content in iPSC-derived neurons increased the baseline membrane lipid packing, explained by an increase in molecular density in the membrane bilayer. Applying strain to cholesterol-loaded cells also caused a fluidization effect (decrease in lipid packing), though smaller than that observed in control cells (Fig. 5). Cholesterol addition to lipid membranes has previously been shown to alter membrane mechanical properties, increasing storage and loss moduli (Al-Rekabi and Contera, 2018) and stiffness (Needham and Nunn, 1990), explaining the smaller decrease in lipid packing measured during stretch and showing how the addition of cholesterol modulates the mechanical properties of the cell membrane.

Lipid packing and membrane fluidity have been previously linked with neural activity. Anaesthetizing agents such as ketamine (Jerabek et al., 2010) and alcohols (Sun and Sun, 1985) are known to alter synaptic and electrophysiological function of neurons by altering membrane lipid conformation and mechanical properties. C-Laurdan imaging results provide evidence that the cell membrane structural properties are being altered during stretch, and that cholesterol addition mitigates this effect by altering the membrane mechanical properties.

### Alterations in Spontaneous Activity

Calcium imaging is a well-established technique used to indirectly record neural activity by imaging changes in intracellular calcium caused by synaptic activity. Fast spiking, caused by rapid calcium influx and efflux due to synaptic stimuli and AP propagation can be used to monitor electrophysiological activity (Jimbo et al., 1993) and connectivity in cultured neurons (Grienberger and Konnerth, 2012). Here, we used fast calcium spiking to assess the effect of changing membrane mechanical properties by cholesterol addition on spontaneous electrophysiology of human iPSC-derived neurons within mature cultures during and after uniaxial strain.

Our results indicate that the onset of damage occurs immediately during stretch. The number of active cells decreased linearly with increasing applied strain and no immediate activity recovery was observed following release of strain (Fig. 6B). Spike analysis further revealed a significant increase in rise and fall time, indicative of impaired calcium dynamics (Grienberger and Konnerth, 2012). This could be a result of a non-selective ion influx due to membrane mechanoporation, which has been shown to occur in rat cortical neurons both under shear flow (Prado et al., 2005) and equibiaxial strain (Geddes et al., 2003) as well as *in vivo* (Petus et al., 1994; LaPlaca et al., 2018). However, rapid re-

sealing of membranes has been observed after injury (Prado et al., 2005), and would suggest a short-term recovery not seen here. Furthermore, our observations of reduced spiking per active cell and altered rise and fall time point to impaired mechanisms of ion influx and efflux, rather than a large immediate non-selective influx caused by membrane poration that would result in a long-term rise in intracellular calcium. Recent computational and experimental work has shown that ion channel damage is a necessary factor to explain the decrease in action potentials caused by neuron strain (Kwong et al., 2019). This suggests that strain causes damage to the ion channels and synapses at the cell membrane, altering their dynamic behavior, in turn altering neuron spontaneous activity.

Strain has also been shown to decrease AP firing frequency, and increase spike interval in neurons cultured on multi-electrode arrays (Prado et al., 2005). In both cases, loss of spontaneous activity was attributed to a combination of damaged synaptic connectivity and membrane structural changes. Post-synaptic currents have also been shown to decrease in rat cortical neurons following stretch; further evidence that strain results in aberrant connectivity between neurons (Goforth et al., 2011; Witgen et al., 2005). Interestingly, developmental stretch (strain rates of 1 mm/day, approximately  $0.5 \times 10^{-5} \text{ s}^{-1}$ ), has been shown not to alter real-time calcium spiking and AP firing, suggesting an active growth process occurring faster than damage and that synaptic connections are maintained if neurons are stretched at low strain rates (Loverde and Pfister, 2015). At very low strain rates, it is possible that the cell membrane undergoes an adaptive process, thereby limiting the changes in its mechanical state. At higher strain rates such as those used here and in literature, the abrupt alteration in membrane mechanical state due to strain causes immediate changes in single cell activity and synaptic connectivity, reducing spontaneous activity. Although reports detailing the effect of different strain rates on neural injury vary, most results show that non-developmental strain rates as high as  $30 \text{ s}^{-1}$  (Magou et al., 2015), and as low as  $0.008 \text{ s}^{-1}$  (Shi and Whitebone, 2006) produce a damaging effect on neural activity. Studies on hippocampal organotypic cultures subject to stretch injury have shown that strain, rather than strain rate, is the determining factor relating injury to cell death (Cater et al., 2006). Overall, the loss of spontaneous activity with applied strain is likely due to an interaction of multiple factors, including alterations of individual cell electrophysiology combined with aberrant synaptic communication. Our results show that the onset of dysfunction occurs immediately with strain application, and exacerbates with increasing strain magnitude. This short timeframe points to direct mechanical damage, rather than a secondary process, as being the cause of dysfunction.

Cholesterol is a primary component of the cell membrane making up 50% of membrane molar fraction, and is crucial in membrane organization and physiological function (Schroeder et al., 1995). Altering the membrane mechanical properties by cholesterol addition did not change the percentage of active cells (Fig. 6A), indicating that cholesterol addition does not interfere with cell spontaneous activity.

Increased cholesterol significantly reduced the severity of the decrease in spontaneous calcium spiking caused by strain (Fig. 6E). Spike rise and fall times for cholesterol-enriched cells were not affected by strain, while in control cells strain increased average rise and fall time (Fig. 6C and D).

Our results show that cholesterol addition increases cell membrane lipid packing suggesting that it alters cell membrane mechanical properties, and reduces the decrease in membrane lipid packing caused by applied strain. GP measurements from Laurdan (a predecessor to c-Laurdan) have been shown to vary linearly with membrane tension and reduce with increased tension (Zhang et al., 2006), suggesting that the reduced decrease in GP observed here in cholesterol-enriched cells is dependent on the mechanical properties of the membrane itself. Membrane stiffness has been shown to increase with cholesterol addition (Needham and Nunn, 1990) and decrease with cholesterol depletion (Vlahakis et al., 2002). Gramicidin channels, widely used as molecular membrane force transducers, have also been used to show molecular stiffening in cholesterol-enriched membranes (Lundbæk et al., 1996), indicating that the reduced effect of strain on lipid unpacking could be caused by an increase in membrane stiffness due to cholesterol addition.

This change in membrane properties with cholesterol addition results in a reduction of the effect of strain on spontaneous neural activity, decreasing the loss of synaptic connectivity and alleviating the effect of stretch on mechanisms regulating ion influx and efflux. In neural membranes, depletion of cholesterol has been shown to increase lateral mobility of fluorescent lipid probe molecules (Pucadyil and Chattopadhyay, 2006), which suggests a decrease in molecular packing similar to what we observed by c-Laurdan imaging in strained neurons (Fig. 5). Neural activity and membrane cholesterol content have been directly linked by Guo et al., concluding that cholesterol levels can bidirectionally modify rat hippocampal primary neuron excitability by modulating ion currents (Guo et al., 2008). Furthermore, depletion of cholesterol in presynaptic terminals has been shown to block evoked synaptic transmission (Koudinov and Koudinova, 2001; Zamir and Charlton, 2006), similarly to how stretch decreases excitatory post-synaptic currents (Goforth et al., 2011). Membrane stiffening by increasing cholesterol content could therefore act to protect the action potential (AP) firing mechanisms in neurons by reducing the mechanical stress applied to ion channels during membrane stretch. Visco-elastic lipid bilayer properties have also been shown to depend on cholesterol content. Forces in neural membranes are regulated by three moduli: compression, area expansion and bending (Tyler, 2012). Increases in membrane moduli would lead to greater resistance to deformation, in turn diminishing the effect of strain on ion channels and synapses. Recently, Al-Rekabi and Contera have shown that increasing the cholesterol molar fraction of artificial lipid bilayers increases the storage and loss modulus, suggesting that cholesterol enrichment leads to increased energy dissipation properties in lipid membranes (Al-Rekabi and Contera, 2018). A greater energy dissipation

would therefore lead to reduced mechanical stress on ion channel mechanisms and synapses, protecting neural functionality. These results, together with the well-established sensitivity of most transmembrane proteins to membrane stretch (Anishkin et al., 2014), indicate that altering membrane mechanical properties lessens the damaging effects of strain on spontaneous activity, highlighting the crucial role of membrane mechanical properties on ion channel and synaptic function, supporting our hypothesis that acute stretch causes aberrant neural activity by altering the mechanical state of the membrane.

This study still presents some limitations that will be tackled in the near future. The mechanical parameters tested were not an extensive representation of injury, and the effect of different strain rates, as well as smaller strain increments, should be used to provide more information about injury mechanisms. Evaluating the recovery of activity after smaller strains could establish a threshold value after which the loss of activity becomes irreversible. In order to further quantify the effect of strain on spontaneous activity, higher frequency imaging can be used to evaluate network connectivity changes as a result of strain as well as the effect of cholesterol addition. By measuring the changes in connectivity and network activity, the impairment of synaptic activity can be differentiated from changes in the activity of the individual cells within the network.

Another limitation of this study is the focus on membrane processes, without investigating the role of cytoskeletal elements in the electrophysiological response to stretch. In future studies, pharmacological cytoskeletal manipulation will be investigated as a factor influencing electrophysiological response during stretch. At the membrane level, we do not directly measure the membrane properties during stretch and as a result of cholesterol addition, but instead rely on GP measurement. Direct elastic and visco-elastic mechanical characterization of cholesterol-enriched neurons, for example by AFM, would provide stronger evidence of changes in membrane mechanical properties.

Overall, the aim of this study was to investigate changes in spontaneous activity properties of human iPSC-derived neurons subject to mechanical stretch. To the best of our knowledge, the experiments reported here are the first spontaneous electrophysiological measurements of human iPSC-derived neurons during strain applied by substrate deformation. Compared to primary rodent cells, overwhelmingly used in *in vitro* studies of neural injury, the use of human iPSC-derived neurons provides a physiologically relevant model, increasing the translational significance of the results.

In summary, we have shown that spontaneous activity of human iPSC-derived neuron networks decreases linearly with applied uniaxial stretch, indicating dysfunction of synaptic connections and of AP firing mechanisms. To understand the importance of cell membrane mechanical properties, c-Laurdan imaging was used to show that cell stretch decreases membrane lipid packing. Cholesterol addition to neural membranes reduces lipid packing decrease during strain, and reduced the loss in spontaneous activity caused by strain. Together these results indicate that the mechanism whereby cell injury causes impaired transmission of neural



impulses is governed by the mechanical state of the cell membrane. This can help understand the onset of nerve conduction blocks, impacting preventive and treatment strategies for mechanical trauma.

## ACKNOWLEDGMENTS

Authors acknowledge China Regenerative Medicine Limited (CRMI) for funding and the EPSRC DTP (award number 1514540) for funding F.B. The authors declare no competing financial interests.

## REFERENCES

- Al-Rekabi Z, Contera S. (2018) Multifrequency AFM reveals lipid membrane mechanical properties and the effect of cholesterol in modulating viscoelasticity. *S A* 115(11):2658-2663.
- Anishkin A, Loukin SH, Teng J, Kung C. (2014) Feeling the hidden mechanical forces in lipid bilayer is an original sense. *S A* 111(22):7898-7905.
- Aron M, Browning R, Carugo D, Sezgin E, Bernardino de la Serna J, Eggeling C, Stride E. (2017) Spectral imaging toolbox: segmentation, hyperstack reconstruction, and batch processing of spectral images for the determination of cell and model membrane lipid order. *BMC Bioinformatics* 18(1):254.
- Bain AC, Meaney DF. (2000) Tissue-level thresholds for axonal damage in an experimental model of central nervous system white matter injury. *J Biomech Eng* 122(6):615-622.
- Barrantes FJ. (2004) Structural basis for lipid modulation of nicotinic acetylcholine receptor function. *Brain Res Rev* 47(1):71-95.
- Bianchi F, Malboubi M, Li Y, George JH, Jerusalem A, Szele F, Thompson MS, Ye H. (2018) Rapid and efficient differentiation of functional motor neurons from human iPSC for neural injury modelling. *Stem Cell Res* 32:126-134.
- Brohawn SG, Su Z, MacKinnon R. (2014) Mechanosensitivity is mediated directly by the lipid membrane in TRAAK and TREK1 K<sup>+</sup> channels. *S A* 111(9):3614-3619.
- Cater HL, Sundstrom LE, Morrison B. (2006) Temporal development of hippocampal cell death is dependent on tissue strain but not strain rate. *J Biomech* 39(15):2810-2818.
- Christian AE, Haynes MP, Phillips MC, Rothblat GH. (1997) Use of cyclodextrins for manipulating cellular cholesterol content. *J Lipid Res* 38(11):2264-2272.
- Geddes DM, Cargill RS, LaPlaca MC. (2003) Mechanical stretch to neurons results in a strain rate and magnitude-dependent increase in plasma membrane permeability. *J Neurotrauma* 20(10):1039-1049.
- Gilchrist CL, Witvoet-Braam SW, Guilak F, Setton LA. (2007) Measurement of intracellular strain on deformable substrates with texture correlation. *J Biomech* 40(4):786-794.
- Goforth PB, Ren J, Schwartz BS, Satin LS. (2011) Excitatory synaptic transmission and network activity are depressed following mechanical injury in cortical neurons. *J Neurophysiol* 105(5):2350-2363.
- Grienberger C, Konnerth A. (2012) Imaging calcium in neurons. *Neuron* 73(5):862-885.
- Guo J, Chi S, Xu H, Jin G, Qi Z. (2008) Effects of cholesterol levels on the excitability of rat hippocampal neurons. *Mol Membr Biol* 25(3):216-223.
- Jerabek H, Pabst G, Rappolt M, Stockner T. (2010) Membrane-mediated effect on ion channels induced by the anesthetic drug ketamine. *J Am Chem Soc* 132(23):7990-7997.
- Jimbo Y, Robinson HP, Kawana A. (1993) Simultaneous measurement of intracellular calcium and electrical activity from patterned neural networks in culture. *IEEE Trans Biomed Eng* 40(8):804-810.
- Koudinov AR, Koudinova NV. (2001) Essential role for cholesterol in synaptic plasticity and neuronal degeneration. *FASEB J* 15(10):1858-1860.
- Kwong MT, Bianchi F, Malboubi M, García-Grajales JA, Homsí L, Thompson M, Ye H, Noels L, Jérusalem A. (2019) 3D finite element formulation for mechanical–electrophysiological coupling in axonopathy. *Comput Methods Appl Mech Eng* 346:1025-1050.
- Laitko U, Juranka PF, Morris CE. (2006) Membrane stretch slows the concerted step prior to opening in a K<sup>+</sup> channel. *J Gen Physiol* 127(6):687-701.
- LaPlaca MC, Lessing MC, Prado GR, Zhou R, Tate CC, Geddes-Klein D, Meaney DF, Zhang L. (2018) Mechanoporation is a potential indicator of tissue strain and subsequent degeneration following experimental traumatic brain injury. *Clin Biomech*. pii: S0268-0033(18)30476-5.
- Levitan I, Fang Y, Rosenhouse-Dantsker A, Romanenko V. (2010) Cholesterol and ion channels. *Cholesterol Binding and Cholesterol Transport Proteins*, volume 51 of *Subcellular Biochemistry*. Dordrecht: Springer. p. 509-549.
- Loverde JR, Pfister BJ. (2015) Developmental axon stretch stimulates neuron growth while maintaining normal electrical activity, intracellular calcium flux, and somatic morphology. *Front Cell Neurosci* 9:308.
- Lundbæk JA, Birn P, Girshman J, Hansen AJ, Andersen OS. (1996) Membrane stiffness and channel function. *Biochemistry* 35(12):3825-3830.
- Lundbaek JA, Birn P, Hansen AJ, Søgaard R, Nielsen C, Girshman J, Bruno MJ, Tape SE, Egebjerg J, Greathouse DV, Mattice GL, Koeppe RE, Andersen OS. (2004) Regulation of sodium channel function by bilayer elasticity: the importance of hydrophobic coupling. Effects of micelle-forming amphiphiles and cholesterol. *J Gen Physiol* 123(5):599-621.
- Magou GC, Pfister BJ, Berlin JR. (2015) Effect of acute stretch injury on action potential and network activity of rat neocortical neurons in culture. *Brain Res* 1624(Supplement C):525-535.
- Morris CE, Prikryl EA, Joós B. (2015) Mechanosensitive gating of K<sup>+</sup> channels. *PLoS One* 10(2):e0118335.
- Needham D, Nunn RS. (1990) Elastic deformation and failure of lipid bilayer membranes containing cholesterol. *Biophys J* 58(4):997-1009.
- Ng LJ, Volman V, Gibbons MM, Phohomsiri P, Cui J, Swenson DJ, Stuhmiller JH. (2017) A mechanistic end-to-end concussion model that translates head kinematics to neurologic injury. *Front Neurol* 8.
- Pereno V, Carugo D, Bau L, Sezgin E, Bernardino de la Serna J, Eggeling C, Stride E. (2017) Electroformation of giant unilamellar vesicles on stainless steel electrodes. *ACS Omega* 2(3):994-1002.
- Pettus EH, Christman CW, Giebel ML, Povlishock JT. (1994) Traumatically induced altered membrane permeability: its relationship to traumatically induced reactive axonal change. *J Neurotrauma* 11(5):507-522.
- Phillips R, Ursell T, Wiggins P, Sens P. (2009) Emerging roles for lipids in shaping membrane-protein function. *Nature* 459(7245):379-385.
- Prado GR, Ross JD, DeWeerth SP, LaPlaca MC. (2005) Mechanical trauma induces immediate changes in neuronal network activity. *J Neural Eng* 2(4):148-158.
- Pucadyil TJ, Chattopadhyay A. (2006) Effect of cholesterol on lateral diffusion of fluorescent lipid probes in native hippocampal membranes. *Chem Phys Lipids* 143(1–2):11-21.
- Qi Y, Andolfi L, Frattini F, Mayer F, Lazzarino M, Hu J. (2015) Membrane stiffening by STOML3 facilitates mechanosensation in sensory neurons. *Nat Commun* 6:8512.
- Rickett T, Connell S, Bastijanic J, Hegde S, Shi R. (2011) Functional and mechanical evaluation of nerve stretch injury. *J Med Syst* 35(5):787-793.
- Schroeder F, Woodford JK, Kavecansky J, Wood WG, Joiner C. (1995) Cholesterol domains in biological membranes. *Mol Membr Biol* 12(1):113-119.
- Sezgin E, Sadowski T, Simons K. (2014) Measuring lipid packing of model and cellular membranes with environment sensitive probes. *Langmuir* 30(27):8160-8166.
- Sezgin E, Waithe D, Bernardino de la Serna J, Eggeling C. (2015) Spectral imaging to measure heterogeneity in membrane lipid packing. *Chemphyschem* 16(7):1387-1394.
- Sharp DJ, Scott G, Leech R. (2014) Network dysfunction after traumatic brain injury. *Nat Rev Neurol* 10(3):156-166.
- Shi R, Whitebone J. (2006) Conduction deficits and membrane disruption of spinal cord axons as a function of magnitude and rate of strain. *J Neurophysiol* 95(6):3384-3390.
- Simons TJB. (1988) Calcium and neuronal function. *Neurosurg Rev* 11(2):119-129.

- Singh S, Pelegri AA, Shreiber DI. (2017) Estimating axonal strain and failure following white matter stretch using contactin-associated protein as a fiduciary marker. *J Biomech* 51:32–41.
- Smetters D, Majewska A, Yuste R. (1999) Detecting action potentials in neuronal populations with calcium imaging. *Methods* 18(2):215–221.
- Spector AA, Yorek MA. (1985) Membrane lipid composition and cellular function. *J Lipid Res* 26(9):1015–1035.
- Sun GY, Sun AY. (1985) Ethanol and membrane lipids. *Alcohol Clin Exp Res* 9(2):164–180.
- Thévenaz P, Delgado-Gonzalo R, Unser M. (2011) The ovuscul. *IEEE Trans Pattern Anal Mach Intell* 33(2):382–393.
- Tillman TS, Cascio M. (2003) Effects of membrane lipids on ion channel structure and function. *Cell Biochem Biophys* 38(2):161–190.
- Tyler WJ. (2012) The mechanobiology of brain function. *Nat Rev Neurosci* 13(12):867–878.
- Vlahakis NE, Schroeder MA, Pagano RE, Hubmayr RD. (2002) Role of deformation-induced lipid trafficking in the prevention of plasma membrane stress failure. *Respir Crit Care Med* 166(9):1282–1289.
- Wall ME, Weinhold PS, Siu T, Brown TD, Banes AJ. (2007) Comparison of cellular strain with applied substrate strain in vitro. *J Biomech* 40(1):173–181.
- Wang JA, Lin W, Morris T, Banderali U, Juranka PF, Morris CE. (2009) Membrane trauma and Na<sup>+</sup> leak from Nav1.6 channels. *Physiol Cell Physiol* 297(4):C823–C834.
- Wei W.-C., Bianchi F, Wang Y.-K., Tang M.-J., Ye H, Glitsch MD. (2018) Coincidence detection of membrane stretch and extracellular pH by the proton-sensing receptor OGR1 (GPR68). *Curr Biol* 28(23):3815–3823.
- Witgen BM, Lifshitz J, Smith ML, Schwarzbach E, Liang S.-L., Grady MS, Cohen AS. (2005) Regional hippocampal alteration associated with cognitive deficit following experimental brain injury: a systems, network and cellular evaluation. *Neuroscience* 133(1):1–15.
- Yamamoto K, Ando J. (2013) Endothelial cell and model membranes respond to shear stress by rapidly decreasing the order of their lipid phases. *J Cell Sci* 126(Pt 5):1227–1234.
- Yamamoto K, Ando J. (2015) Vascular endothelial cell membranes differentiate between stretch and shear stress through transitions in their lipid phases. *Physiol Heart Circ Physiol* 309(7):H1178–H1185.
- Yang Y.-T., Liao J.-D., Lin C.-C.K., Chang C.-T., Wang S.-H., Ju M.-S.. (2011) Characterization of cholesterol-depleted or -restored cell membranes by depth-sensing nano-indentation. *Soft Matter* 8(3):682–687.
- Zamir O, Charlton MP. (2006) Cholesterol and synaptic transmitter release at crayfish neuromuscular junctions. *J Physiol* 571(Pt 1):83–99.
- Zhang Y.-L., Frangos JA, Chachisvilis M. (2006) Laurdan fluorescence senses mechanical strain in the lipid bilayer membrane. *Biochem Biophys Res Commun* 347(3):838–841.
- Zidovetzki R, Levitan I. (2007) Use of cyclodextrins to manipulate plasma membrane cholesterol content: evidence, misconceptions and control strategies. *Biochim Biophys Acta* 1768(6):1311–1324.

(Received 11 August 2018, Accepted 11 February 2019)

(Available online 26 February 2019)